Causal Connectivity Network Analysis of Ictal Electrocorticogram With Temporal Lobe Epilepsy Based on Dynamic Phase Transfer Entropy

Yao Miao, Hiroharu Suzuki, Hidenori Sugano, Tetsuya Ueda, Yasushi Iimura, Ryosuke Matsui, and Toshihisa Tanaka, *Senior Member, IEEE*

***Abstract*—Temporallobe epilepsy (TLE) has been conceptualized as a brain network disease, which generates brain connectivity dynamics within and beyond the temporal lobe structures in seizures. The hippocampus is a representative epileptogenic focus in TLE. Understanding the causal connectivity in terms of brain network during seizures is crucial in revealing the triggering mechanism of epileptic seizures originating from the hippocampus (HPC) spread to the lateral temporal cortex (LTC) by ictal electrocorticogram (ECoG), particularly in high-frequency oscillations (HFOs) bands. In this study, we proposed the unified-epoch dynamic causality analysis method to investigate the causal influence dynamics between two brain regions (HPC and LTC) at interictal and ictal phases in the frequency range of 1–500 Hz by introducing the phase transfer entropy (PTE) out/in-ratio and sliding window. We also proposed PTE-based machine learning algorithms to identify epileptogenic zone (EZ). Nine patients with a total of 26 seizures were included in this study. We hypothesized that: 1) HPC is the focus with the stronger causal connectivity than that in LTC in the ictal state at gamma and HFOs bands. 2) Causal connectivity in the ictal phase shows significant changes compared to that in the interictal phase. 3) The PTE out/in-ratio in the HFOs band can identify the EZ with the best prediction performance.**

***Index Terms*—Phase transfer entropy (PTE) out/in-ratio, ictal electrocorticogram (ECoG), epileptogenic zone (EZ) identification, machine learning.**

Manuscript received 4 May 2023; revised 1 August 2023 and 16 August 2023; accepted 22 August 2023. Date of publication 25 August 2023; date of current version 22 January 2024. This work was supported by JST CREST under Grant JPMJCR1784. *(Yao Miao and Hiroharu Suzuki contributed equally to this work.) (Corresponding author: Toshihisa Tanaka.)*

Yao Miao and Ryosuke Matsui are with the Tokyo University of Agriculture and Technology, Japan, and also with the Department of Neurosurgery, Juntendo University School of Medicine, Japan.

Hiroharu Suzuki, Hidenori Sugano, Tetsuya Ueda, and Yasushi Iimura are with the Department of Neurosurgery, Juntendo University School of Medicine, Japan.

Toshihisa Tanaka is with the Tokyo University of Agriculture and Technology, Tokyo 113-8421, Japan, and also with the RIKEN Center for Advanced Intelligence Project, Tokyo 113-8421, Japan (e-mail: tanakat@cc.tuat.ac.jp).

This article has supplementary downloadable material available at https://doi.org/10.1109/TBME.2023.3308616, provided by the authors.

Digital Object Identifier 10.1109/TBME.2023.3308616

I. Introduction

EPILEPSY, one of the most common chronic neurological disorders characterized by unpredictable recurrent seizures, is a typical network disorder [1], [2], [3]. Temporal lobe epilepsy (TLE), which is the most common form of focal epilepsy, is increasingly considered a network disease that leads to brain connectivity change within and without temporal lobe [4], [5], [6], [7]. A growing literature suggests that brain disorders may be related to abnormal connections and brain network instability between connected brain regions [8], [9], [10]. Hence, to advance the therapeutic management of epilepsy, a detailed understanding of connectivity of brain activity is required [11].

Electrocorticography (ECoG) is one of the procedures used for recording brain activity with high spatial and spectral resolution in epilepsy diagnosis [12]. Effective connectivity (EC) refers to the influence of one neural system over the other [13]. It can reveal changes in the connectivity of brain activity in terms of direction and strength. EC is commonly evaluated by the vector autoregressive (VAR) model-based measures such as the Granger causality (GC) score [14], the partial directed coherence (PDC) [15], and the directed transfer function (DTF) [16]. An early study has used the DTF to identify seizure onset zone (SOZ) for the ictal intracranial electroencephalography (iEEG) with mesial temporal seizure based on the analyzed propagation patterns [17]. The follow-up research has proposed the integrated DTF (IDTF) to extend analysis of SOZ localization for the iEEG with seizures originating from both the mesial temporal structures and the lateral temporal neocortex [18]. A different study has applied an extension of the DTF termed as adaptive directed transfer function (ADTF) to the SOZ identification based on electrocorticography (ECoG) interictal spike recorded from the patients with intractable epilepsy [19]. Surveys such as [20], [21] have developed a modified version of the ADTF to localize the ictal onset zone for iEEG with refractory epilepsy. Moreover, one study has performed the GC analysis on the ictal iEEG of the high-frequency band for SOZ localization [22].

However, it is well known that the VAR model is established on the assumption that the signal processed is quasi-stationary [23]. Concerns have been raised about the limitations of EC estimation for non-stationary signals. Recently, the model-free transfer entropy (TE)-based method, the phase

TABLE I
SUMMARY OF INFORMATION FOR NINE PATIENTS

Patient ID	Gender	Age at onset (years)	Age at surgery (years)	Side	Symptom	Pathology	Follow up Month	Engel class	#Seizures	#Hippocampus electrodes	#Lat.Temp. electrodes
Pt1	F	26	41	left	FIAS/automatism	Gliosis	23	Ib	4	4	24
Pt2	F	6	30	left	FIAS/automatism motionless staring	Hippocampal sclerosis	32	Ia	4	4	24
Pt3	M	50	52	left	FIAS/automatism	Amygdala enlarge	50	Ia	1	4	24
Pt4	F	27	41	right	FIAS/automatism	Hippocampal sclerosis	33	Ia	2	4	24
Pt5	M	15	24	right	FIAS	Hippocampal sclerosis	45	Ia	2	4	48
Pt6	M	27	38	left	FIAS/automatism	Hippocampal sclerosis	46	Ia	3	4	24
Pt7	M	56	57	left	FIAS	Amygdala enlarge	55	Ia	6	4	24
Pt8	F	23	28	left	FIAS/automatism	Amygdala enlarge	33	Ia	1	4	24
Pt9	F	20	31	left	FIAS language disturbance	Amygdala enlarge	62	Ic	3	4	24

transfer entropy (PTE), has been proposed to analyze the non-stationary epileptic EEG [24], [25]. In a related study, the PTE and graph theory have been employed to evaluate the stereo-electroencephalography (SEEG) with TLE and detect the epileptogenic zone (EZ) [26]. However, there is little literature on detailed information on how the information flow is transported and what the information flow strength is between selected brain regions before and during seizures for TLE, particularly in high-frequency oscillations (HFOs).

In this article, we proposed the unified-epoch phase transfer entropy (PTE)-based dynamic methods to investigate the time-varying causal connectivity changes of ECoG recordings with TLE seizures among multiple electrodes located in selected brain regions, including the hippocampus (HPC) and the lateral temporal cortex (LTC). In particular, we introduced the PTE out/in-ratio to evaluate the strength of the causal influence to overcome the limitation of the various numbers of electrodes for each patient. Besides, we introduced the unified-epoch approach to address the problem resulting from the time-variance of seizure duration. We employed three machine learning algorithms to distinguish the HPC and LTC electrodes, in which the HPC electrodes analyzed were labeled to EZ by epileptologists. Moreover, we proposed leave-one seizure-out cross-validation (LOSOCV), segment-wise approach, and electrode-wise measure to estimate the identification performance of EZ. In this study, we will demonstrate how PTE-based dynamic measures can be used to estimate the strength and the preferred direction of the information flow between HPC and LTC over the epochs before and during the seizure. We will also test the feasibility of PTE-based machine learning models for EZ identification. We hypothesize that: 1) HPC shows a significant increase in the causal influence from seizure onset, making it toward surrounding structures at gamma and HFOs bands. 2) PTE out/in-ratio at the HFOs band can be a promising biomarker for identifying EZ.

II. MATERIALS AND METHODS

A. Participants

Between June 2014 and December 2019, 36 patients with pharmaco-resistant TLE underwent ECoG using the subdural electrodes before focus resection in Juntendo University Hospital. We selected the ictal ECoG based on the following four inclusion criteria: 1) ictal semiology was focal impaired awareness seizure, suspected to originate from the mesial temporal lobe; 2) seizure onset was found in the HPC with rhythmic spikes or paroxysmal fast activity; 3) Engel's classification of class 1; and 4) the etiologies were not focal cortical dysplasia, brain tumor, vascular disease, or uregria. For analysis, we identified the ictal ECoG data of 26 seizures from nine patients comprising four males and five females to analyze. We conducted a retrospective analysis and obtained data using an opt-in/opt-out method. The registration and analysis were approved by the ethics committee of Juntendo University (16-163), and the study was conducted following the Declaration of Helsinki.

Table I summarizes the information regarding gender, age at onset, age at surgery, side, symptom, pathology, follow-up month, Engel's classification outcome, number of seizures per patient during ECoG recording, and the number of electrodes located in the regions of the HPC and LTC. The age at onset varied from 6 to 56 years, whereas the age at surgery ranged from 24 to 57 years. Hippocampus sclerosis pathology was identified in four patients (44.4%), amygdala enlargement pathology in four patients (44.4%), and gliosis pathology in one patient (11.1%). Seven patients had the outcome of Engel Class Ia, one patient was in Engel Class Ib, and one patient was with Engel Class Ic after the evaluation by Engel's classification of postoperative [27], [28]. Furthermore, the number of seizures for each patient varied from one to six.

B. ECoG Acquisition

The ECoG recordings were acquired using Neuro Fax digital video EEG system (Nihon Kohden, Inc., Tokyo, Japan) with a sampling frequency of 2000 Hz for all nine patients. The number of electrodes for each patient varied, ranging from 40 to 94. The four contacts covering the HPC and 24 contacts covering the LTC regions were selected for the analysis, except for one patient with 48 contacts in the LTC. And there were five LTC electrodes with bad ECoG quality and were not included in this study. In addition, we defined the interictal phase as two minutes before the seizure onset and the ictal phase as from the seizure onset

to the end of the seizure with variant durations of 37 s–100 s (62.31 s±18.71 s). The four selected HPC electrodes are the EZ electrodes, which are the electrodes where the seizure begins.

C. ECoG Preprocessing

Before estimating the characteristics of effective connectivity, we filtered the ECoG signal using the two-way least squares zero-phase finite impulse response (FIR) filter by introducing the function of eegfilt.m from the EEGLAB toolbox and $order = 3 \times fix(Fs/locutoff)$ [29]. To observe the dynamics in a high-frequency resolution, we introduced the narrow bandwidth filtering measure to perform the filtering process. Specifically, the range of 1–80 Hz was divided into 79 subbands by a bandpass filter with a bandwidth of 1 Hz, and that of 80–500 Hz was divided into 84 subbands using a bandpass filter with a bandwidth of 5 Hz. We introduced the frequency response and total harmonic distortion (THD) analysis to assess the performance of the 1 Hz-bandpass FIR filter. The THD was computed using $THD(\%) = \sqrt{\frac{P_{Harmonics}}{P_{Fundamental}}} \times 100$, in which $P_{Harmonics}$ and $P_{Fundamental}$ were the power of harmonic components and the power of fundamental component [30]. Supplementary Fig. S1 demonstrates that the proposed FIR filter exhibits a high amplitude response, a relatively linear phase response, and minimal ripples across each 1 Hz subband within the frequency range of [1 Hz, 80 Hz]. These characteristics indicate that the filter effectively maintains the signal's strength while minimizing distortions in the time-domain representation. Supplementary Fig. S2 further supports the effectiveness of the proposed filter. In Supplementary Fig. S2(A), we present the THD values for each fundamental frequency in the range of [1 Hz, 80 Hz], utilizing the proposed 1 Hz-bandpass filter. The average THD across all fundamental frequencies is reported as 0.059%. This reveals that the filter significantly reduces distortion, resulting in a cleaner and more accurate representation of the signal. Building upon this evidence, Supplementary Fig. S2(B), (C1), and (C2) display the THD values across different electrodes, specifically highlighting the reduction in harmonic components of both a sinusoidal wave and an ECoG data at the specific fundamental frequency of 10.5 Hz. These additional findings provide further support for the effectiveness of the proposed filter. Collectively, these findings indicate that the proposed filter effectively lowers THD levels and produces signals with improved cleanliness and fidelity.

Because the time duration of the ictal phase was case-various, we proposed the approach of unified-epoch with fixed overlap to estimate the chronological changes of features at each band for each seizure. The fixed overlap measure was applied to avoid the non-calculated segment resulting from an inappropriate or small time window size. In this study, the overlap was set to 80%, and the number of epochs was 600 and 185 for each seizure in the interictal and ictal phases, respectively.

D. Phase Transfer Entropy Out/In-Ratio

PTE is a non-parametric, Wiener-Granger Causality principle-based phase-specific directed effective connectivity measure [14], [31], [32]. It explains the improvement of uncertainty in predicting the future of the target signal when the past of both the source signal and target signal are known, compared to when only considering the past of the target signal. The calculation of the PTE for a given past source signal $X(t)$, a past target signal $Y(t)$, and a given delay δ is defined as follows [25], [33]:

$$PTE_{X\to Y}^{(\delta)} = \sum p(\theta_y(t+\delta))p(\theta_y(t))p(\theta_x(t)) \log \frac{p(\theta_y(t+\delta)|\theta_y(t),\theta_x(t))}{p(\theta_y(t+\delta)|\theta_y(t))}, \quad (1)$$

where $\theta_X(t)$, $\theta_Y(t)$, and $\theta_Y(t+\delta)$ are the instantaneous phase time series of $X(t)$, $Y(t)$, and $Y(t+\delta)$, respectively. $p(\theta_x(t))$, $p(\theta_y(t))$, and $p(\theta_y(t+\delta))$ indicate the marginal probability mass function of $\theta_X(t)$, $\theta_Y(t)$, and $\theta_Y(t+\delta)$, respectively. The probabilities are obtained by introducing the histogram method to bin occurrences of single, pairs, or triplets of phase estimates in an epoch [25]. The bin width is defined as $h = 3.49\sigma/N^{\frac{1}{3}}$ based on Scott's approach [34], where h, σ, and N denote the bin width of the phase time series, the standard deviation of a directional variable [35], and the number of sampling points, respectively. The number of histogram bins is therefore set to $2\pi/h$. In addition, the prediction delay δ is also set to the number of times the phase flips across time and electrodes [36]. Because the number of electrodes of the two regions (HPC and LTC) for each patient varies, the PTE out/in-ratio value was employed to evaluate the causal influence from designated source electrodes to target electrodes. The definition of PTE out/in-ratio values is as follows:

$$ratio = \frac{\sum_{j=1,i\neq j}^{N_{ch}} PTE_{i\to j}^{(\delta)}}{\sum_{j=1,j\neq i}^{N_{ch}} PTE_{j\to i}^{(\delta)}}, \quad (2)$$

where $ratio$ denotes the PTE out/in-ratio. N_{ch} indicates the number of electrodes.

This study applied the PTE out/in-ratio method to evaluate the effective connectivity between all pairs of electrodes in the HPC and LTC of each epoch at each narrow band for each seizure. To reduce the numerical instability resulting from our proposed segmentation measure, the moving average filter approach was performed using a smoothing window with 11 points at each narrow frequency band [37]. Owing to the number of electrodes and the location of electrodes being patient-various, we proposed the approach of region-region network analysis to evaluate the dynamics of causal influence between pairs of the region of interest (ROI) along with the time for each seizure. Two ROIs were included in this analysis which were the HPC and LTC, generating two directions, including the direction from HPC to LTC and vice versa. In addition, we computed the direct causal connectivity of the two region-region directions at each narrow frequency band for each seizure. To construct the network connectivity between ROIs for this type of seizure, the out/in-ratio time series of each direction computed based on our proposed method were normalized along with time by calculating the amount of increase and decrease based on the median interictal out/in-ratio values at each band for each seizure

and averaged over seizures for each band. Compared to the mean, the median is less sensitive to extreme values and can be used to minimize the effect of abnormal brain activity. And the median is a nonparametric measure that serves as a reference for a signal. We therefore use median values for normalization in this study. For the designated type of seizure and each of the two directions, the chronological dynamics of the full-frequency network connectivity was graphically represented by a connectogram. In addition, we proposed a node-region analysis measure to investigate the time-variant changes of causal connectivity to investigate the changes in the causal influence exerted by one designated electrode to one given region for an individual case.

E. Statistical Analysis

The non-parametric Mann-Whitney U test was performed to examine the significant difference between the median values in the interictal phase and the transient values in the ictal phase across seizures at each of 785 epoch for each of 163 frequency subbands. The number of samples for each group was 26. p values were set to 0.05, 0.01, and 0.005 to denote significant levels and were represented by hot and cold colors from light to dark in the connectogram. The Kruskal-Wallis H test was applied to compare the classification metrics among the three classifiers. The effect size metric was estimated by common language effect size (CLES) for the Mann-Whitney U test [38]. The eta-squared measure (η_H^2) was computed to evaluate the effect size for the Kruskal-Wallis H test [39]. To mitigate the potential issue of the multiple comparisons problem (MCP) arising from a large number of Mann-Whitney U test comparisons (163×785), we also implemented the false discovery rate (FDR) correction. This correction helps control the increased chance of obtaining false positives and maximizing statistical power when conducting numerous statistical tests simultaneously [40]. Specifically, we applied the Benjamini-Hochberg procedure to adjust the p-values resulting from these statistical tests [41].

F. Classifiers

Three machine learning classifiers, namely light gradient boosting machine (lightGBM), support vector machine (SVM) with radial basis function (RBF) kernel, and SVM with linear kernel, were employed to identify EZ based on the PTE out/in-ratio features. In detail, the normalized PTE out/in-ratio values for all electrodes at each selected frequency band for each epoch were extracted as input. The size of the input of each epoch was $N_{electrode} \times N_{subband}$, in which $N_{electrode}$ and $N_{subband}$ were the number of electrodes and the number of subbands at the selected band. There were a total of 771 electrodes (EZ electrodes: 104, non-EZ electrodes: 667) for all 26 seizures in this study. All the classifiers run on iMac Pro (2017) configured with the processor of Intel Xeon W-2191B.

1) Light Gradient Boosting Machine Model: LightGBM is a state-of-the-art supervised learning model implemented with a novel distributed gradient boosting framework. Gradient-based one-side sampling technology and histogram-based algorithm have been applied in LightGBM. The former improves the model accuracy by focusing on samples with more significant gradients. In contrast, the latter arranges continuous features to discrete bins for acceleration and memory-saving [42]. In addition, the model has been recently applied to detect seizure onset zone in patients with focal cortical dysplasia (FCD) [43], [44], [45]. In this study, we employed the LightGBM Python package to conduct classification based on selected PTE out/in-ratio features for 26 seizures [46]. We set the parameter of class weight to balanced mode to automatically adjust the weight of each class. Besides, we employed a random search for hyperparameter optimization by tuning values of the four crucial parameters: the number of leaves for each tree, the boosting learning rate, the minimal number of data in one leaf, and the maximum tree depth. The values of these four parameters were set to [35, 40, 45, 50, 55, 60, 65], [0.01, 0.05, 0.1, 0.15], [20, 40, 60, 100], and [4, 6, 8, 10], respectively.

2) Support Vector Machine Model: SVM is a supervised machine learning model that uses a kernel function to project features on a high-dimensional feature space and selects the optimal hyperplane in feature space to distinguish samples of binary-class effectively [47]. It has been applied to detect SOZ using EEG in related studies [48]. In this study, we employed SVM with two standard kernels, linear and RBF kernels, to identify EZ.

G. Leave-One Seizure-Out Cross-Validation

To obtain a reliable and unbiased evaluation of the model performance, we proposed the LOSOCV to estimate the performance of the PTE out/in-ratio-based machine learning model for EZ identification. This approach involved training a classification model on the PTE out/in-ratio features of 25 seizures and applying the trained model to predict the EZ for the remaining seizure. This process is repeated for each of the 26 seizures, allowing for an estimation of the classification model performance on a per-seizure basis. To uncover potential biases and provide a more comprehensive evaluation of model's performance across different seizure, we employed the LOSOCV and time series nest cross-validation (TSNCV) to assess the accuracy for each seizure. The normalized PTE out/in-ratio time series for all seizures were split into ten folds in TSNCV.

H. Segment-Wise and Electrode-Wise Evaluations

In this study, we introduced a segment-wise evaluation approach to estimate the classification performance over time. Five standard evaluation metrics, namely specificity, sensitivity, precision, F1 score, and area under the curve (AUC), were introduced to measure the performance of EZ identification of each segment for each seizure. The formulas to calculate the metrics were as follows:

$$Sensitivity = \frac{TP}{TP + FN}, \tag{3}$$

$$Specificity = \frac{TN}{TN + FP}, \tag{4}$$

$$Precision = \frac{TP}{TP + FP}, \tag{5}$$

$$F1\ score = \frac{2TP}{2TP + FP + FN}, \tag{6}$$

$$FPR = \frac{FP}{FP + TN}, \tag{7}$$

where true positive (TP), false positive (FP), true negative (TN), and false negative (FN) denoted the number of correctly identified EZ electrodes from all EZ electrodes, the number of correctly identified non-EZ electrodes from all non-EZ electrodes, the number of incorrectly identified EZ electrodes from all EZ electrodes, and the number of incorrectly identified non-EZ electrodes from all non-EZ electrodes for each segment, respectively. AUC was the area under the curve of sensitivity against the FPR at various threshold settings.

For individual seizures, we proposed the electrode-wise evaluation measure to assess whether one electrode was EZ or not at each segment to observe the prediction performance of each electrode. We used 1 and 0 to represent electrodes with the actual labels with EZ and non-EZ, respectively. The electrode was identified as EZ when the prediction label returned to 1 and displayed yellow. In contrast, the electrode was identified as non-EZ when the prediction label returned to 0 and displayed purple, shown in Supplementary Fig. S7.

III. Results

A. Dynamic Global Out/In-Ratio Patterns (Interictal vs Ictal)

Owing to the duration of the ictal phase being variant with the range of duration of 37 s–100 s, to illustrate the global causal connectivity dynamics for all seizures, we estimated the strength and direction of the causal influence between the HPC and the LTC for all the 26 seizures by employing the region-region unified-epoch PTE-based analysis approach and normalized measure. Firstly, we estimated the PTE out/in-ratio of two directions (HPC→ LTC and LTC→ HPC) of each epoch for each seizure. Then, we established the causality patterns of the two directions for the type of seizure at each band by averaging out/in-ratio cross seizures along with time, resulting in a single dynamic evaluation of the preferred direction of out/in-ratio. We showed the causality patterns by a connectogram, in which the horizontal axis, vertical axis, hot color, and cold color denote the time range, frequency range, directed causal connectivity increase compared to interictal phase, and directed causal connectivity decrease when compared to that in the interictal phase, respectively.

As described in Fig. 2 and Supplementary Fig. S3, in all 26 seizures, a significant increase of the out/in-ratio is found in a wide range of high-frequency bands (gamma, ripple, and fast ripple bands) from HPC to LTC ($p<0.005$, CLES>0.2), whereas a decrease in the frequency range of 10–30 Hz ($p<0.005$, CLES>0.7), compared with the average values at the interictal phase (Fig. 2 (A1) and (B1), Supplementary Fig. S3(A1)). In addition, a significant increase in the out/in-ratio driven by HPC is preceding in the preictal phase (the last interictal spike) before seizure onset in the fast ripple band (Fig. 2 (B1)). This significant increases originating from HPC spread to almost all the frequency bands in the termination of seizures. However, a significant decrease in the out/in-ratio is found in the direction from LTC to HPC above 30 Hz ($p<0.005$, CLES>0.7). In the range of 10–30 Hz, the out/in-ratio sending by LTC demonstrates a significant increase from seizure onset to the middle of seizures ($p<0.005$, CLES>0.7) (Fig. 2 (A2) and (B2), Supplementary Fig. S3(A2)).

We applied the Benjamini-Hochberg procedure to adjust the p-values obtained from the above numerous Mann-Whitney U tests to control FDR when conducting multiple comparisons. As displayed in Supplementary Fig. S4, we observed significant differences between the interictal and ictal phases in most of the HFOs bands ($p<0.005$, CLES>0.7). These results provide strong evidence for the presence of meaningful effects. However, upon examining the adjusted p-values, we found that the significance levels for the differences in the gamma band were reduced compared to the uncorrected p-values.

B. Results of Classification

It is observed from Fig. 2 that there are profound, significant differences in the PTE out/in-ratio between HPC and LTC in the ictal phase at gamma, ripple, and fast ripple bands. This study proposed a PTE-based LightGBM classification model and the LOSOCV to distinguish EZ and non-EZ in the ictal phase at the three bands for all 26 seizures. Five metrics (AUC, sensitivity, specificity, precision, and F1 score) were used to evaluate classification performance. The mean and standard deviation values show the results. Table II summarizes the average classification results using LightGBM and LOSOCV based on the PTE out/in-ratio features at the three bands for all 26 seizures. The results were obtained by taking averages across all 26 seizures and all segments in the ictal phase. The result illustrates that the evaluation values at the fast ripple band in the ictal phase are the highest compared to those at gamma and ripple bands. The AUC, sensitivity, specificity, precision, and F1 score values are 0.883, 0.876, 0.869, 0.732, and 0.772, respectively. Furthermore, using three models, we employed the box and swarm plot measures to present the five classification metrics of 26 leave-one-seizure-out tests in three bands. Furthermore, we performed the Kruskal-Wallis H and Mann-Whitney U tests to evaluate the significant statistics. As displayed in Supplementary Fig. S5, there is statistically different among the three models using the metrics of AUC ($p<0.05$, $\eta_H^2 = 0.058$), sensitivity ($p<0.05$, $\eta_H^2 = 0.139$), and F1 score ($p<0.05$, $\eta_H^2 = 0.071$) in gamma band and using the specificity in ripple band ($p<0.05$, $\eta_H^2 = 0.106$), particularly between the LightGBM and the SVM with linear kernel models based on the metrics of AUC ($p<0.05$, CLES$=0.697$), sensitivity ($p<0.05$, CLES$=0.788$), and F1 score ($p<0.05$, CLES$=0.717$) in gamma band and based on the specificity in ripple band ($p<0.05$, CLES$=0.700$). It is significant different between the SVM with linear kernel and the SVM with RBF kernel models based on sensitivity ($p<0.05$, CLES$=0.340$) in gamma band and based on F1 score ($p<0.05$, CLES$=0.374$) in ripple band. In contrast, no statistical difference is found in the HFOs bands among the three models.

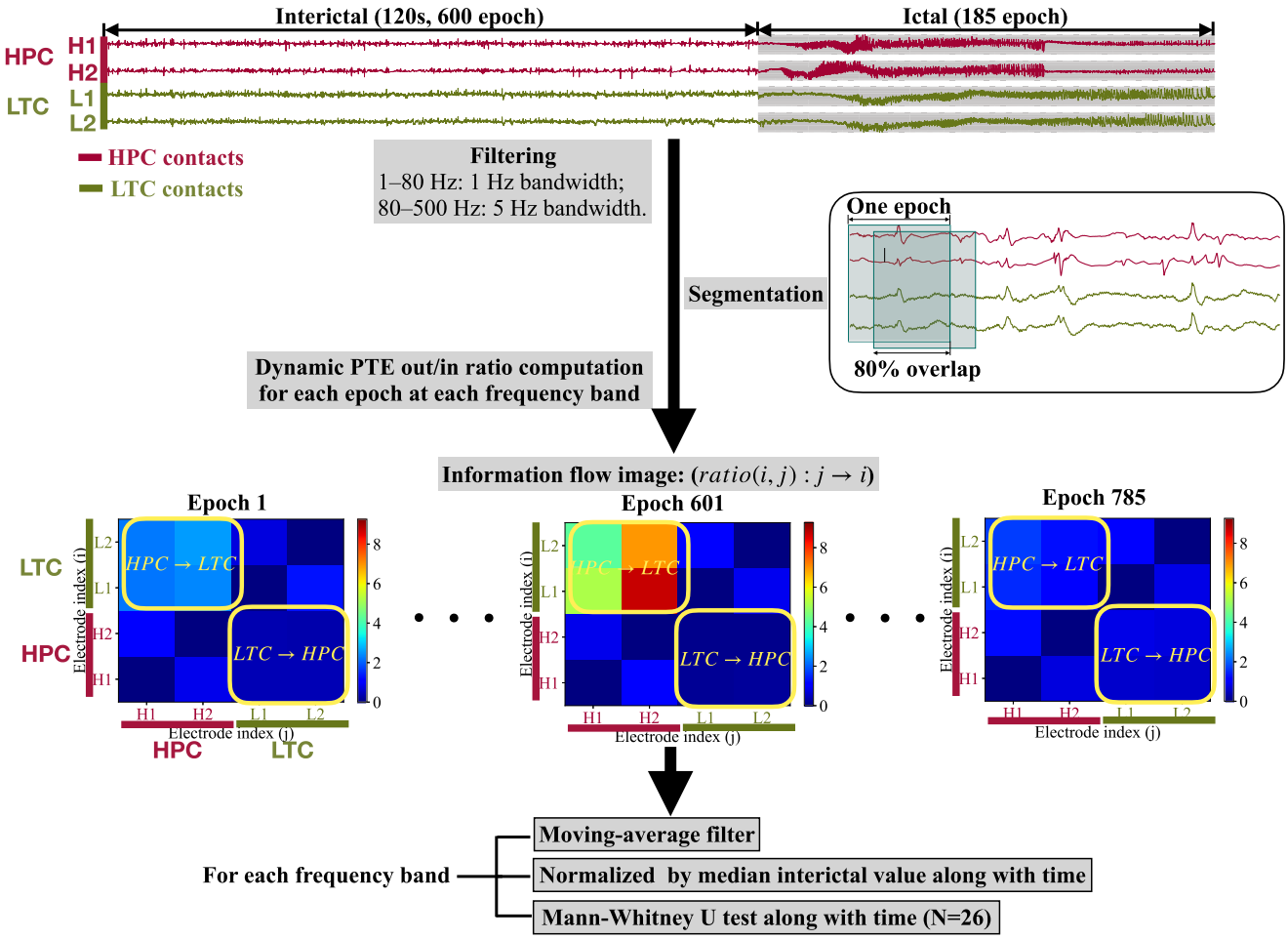

Fig. 1. Scheme of unified-epoch dynamic PTE analysis method for ECoG with TLE. The upper figure presents the raw ECoG recordings during seizures, including the interictal phase with two minutes and the ictal phase from the onset to the end. The lines colored brown and green denote the ECoG recordings located in the HPC and LTC, respectively. There are three steps for analysis, comprising filtering, segmentation, and dynamic PTE out/in-ratio computation approach. The ECoG in the interictal phase (120 s) and ictal phase (37–100 s) were divided into 600 and 185 epochs by the data-based time window with 80% overlap, respectively. The lower figures indicate the information flow images series using region-region unified-epoch PTE-based dynamic analysis measure. The x-axis and y-axis represent the electrode index, and the deep red color denotes the higher PTE out/in-ratio value in the information flow image. ratio(i, j) represents the information flow from electrode j to electrode i. The parts circled by a yellow rectangle present the ratio part with two directions of HPC $\rightarrow$ LTC and LTC $\rightarrow$ HPC, representing the direction from HPC to LTC and the direction from LTC to HPC, respectively.

TABLE II
CLASSIFICATION RESULTS USING THREE MACHINE LEARNING ALGORITHMS AND LOSOCV IN ICTAL PHASE FOR ALL 26 SEIZURES

Band	Method	AUC	Sensitivity	Specificity	Precision	F1 score
Gamma (30–80 Hz)	LightGBM	0.757±0.167	0.752±0.116	0.748±0.164	0.532±0.187	0.582±0.176
	[1]SVM$_{RBF}$	0.708±0.182	0.661±0.202	0.716±0.146	0.473±0.209	0.518±0.210
	[2]SVM$_{Linear}$	0.621±0.203	0.569±0.176	0.641±0.169	0.415±0.188	0.433±0.179
Ripple (80–250 Hz)	LightGBM	0.828±0.147	0.795±0.098	0.823±0.152	0.641±0.179	0.677±0.166
	SVM$_{RBF}$	0.827±0.171	0.760±0.187	0.839±0.143	0.639±0.207	0.665±0.205
	SVM$_{Linear}$	0.770±0.173	0.736±0.155	0.735±0.156	0.558±0.182	0.595±0.174
Fast ripple (250–500 Hz)	LightGBM	**0.883±0.129**	**0.876±0.100**	**0.869±0.127**	**0.732±0.165**	**0.772±0.151**
	SVM$_{RBF}$	0.871±0.144	0.852±0.140	0.850±0.145	0.714±0.191	0.755±0.177
	SVM$_{Linear}$	0.856±0.153	0.839±0.149	0.848±0.146	0.727±0.194	0.760±0.182

[1]SVM$_{Linear}$ is the model of SVM with the linear kernel.
[2]SVM$_{RBF}$ is the model of SVM with the RBF kernel.
The number in bold represents the highest value of each performance metric.

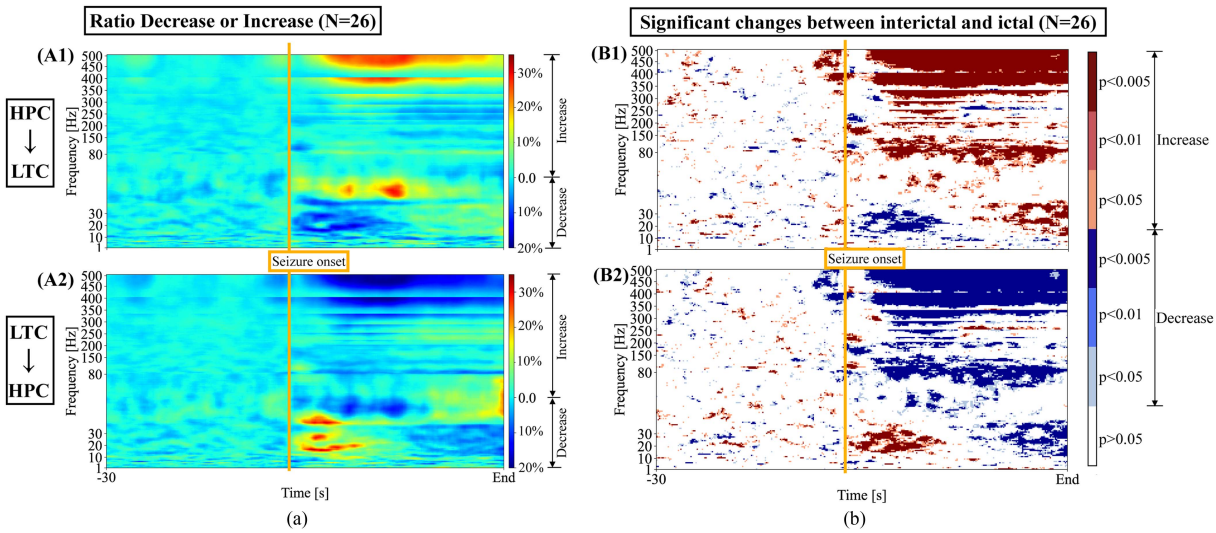

Fig. 2. Average normalized PTE out/in-ratio and significant changes of two directions over time for 26 seizures at full frequency bands with the range of 1–500 Hz. X-axis denotes the time for interictal and ictal phases, and the y-axis represents the frequency band. HPC → LTC and LTC → HPC represent the out/in-ratio direction from HPC to LTC and from LTC to HPC, respectively. The orange line denotes the time points of seizure onset. (A1) and (A2) are the average normalized dynamic PTE out/in-ratio of 26 seizures for the two directions. Hot and cold colors denote the increase and decrease values, respectively. (B1) and (B2) are the dynamic significant changes between the interictal and ictal phases at full frequency bands for the two directions, respectively. Hot and cold colors denote the significant causality increase and decrease, respectively. The significant levels are set to 0.05, 0.01, and 0.005. Colors from light to dark represent different significant levels.

We subsequently examined the accuracy of EZ identification using LOSOCV and TSNCV at the fast ripple band in the ictal phase for each of the 26 seizures. As shown in Supplementary Table SI, the model performance using LOSOCV shows higher model performance with an average accuracy of 0.871. The accuracy of multiple seizures within a given patient such as Pt5 and Pt6 shows similarity using two cross-validation (CV) measures.

Moreover, to provide a more comprehensive evaluation of the proposed EC approach, we compared the performance between the proposed PTE out/in-ratio and the common DTF method, using the ECoG data and machine learning models that were previously used to evaluate the proposed PTE out/in-ratio. As shown in Supplementary Table SII, the classification metric values of DTF are lower than those of the proposed EC approach.

Furthermore, to examine the impact of different overlap values on the classification results of the proposed method, two more overlap values (60% and 40%) were introduced to conduct the same analysis process. The obtained results were used to compare with the classification results using overlap of 80% in each of three bands (gamma, ripple, and fast ripple). The Kruskal-Wallis H test was employed to test the statistical significant differences of AUC and F1 values among the three overlap values. As shown in Supplementary Fig. S6, there is no significant difference among three overlap values, suggesting that the various overlap values may not yield different classification results.

C. Results of Global Chronological Classification

Because epileptic activity in the ictal phase is complex and time-variant, this may cause the classification results to change dynamically over time. Hence, we proposed a segment-wise measure to evaluate the dynamic classification performance along the time window at the fast ripple band for all 26 seizures. As described in Fig. 3, the global trend of classification evaluations shows an increase from seizure onset, then becomes stable during the early seizure stage, and declines slowly from the middle of seizure to the termination of seizure. In particular, the classification performance during the seizure stage from the 37th to the 96th segment, with values almost higher than 0.8 (highlighted by yellow color background), outperforms the remaining segments.

D. Results of Chronological EZ Electrodes Identification for Every Seizure

Results in Fig. 3 have illustrated the global classification performance at the fast ripple band conducted by the LightGBM and LOSOCV based on the PTE out/in-ratio features in the ictal phase. Owing to the case variance in evaluation, we proposed an electrode-wise evaluation measure. We combined it with the segment-wise approach to estimate the chronological prediction performance over the segment at a fast ripple band for each of the 26 seizures. In addition, as displayed in Supplementary Fig. S7, eleven seizures (No.2, No.5, No.11, No.12, N0.13, No.14, No.15, No.18, No.20, No.22, and No.25) achieved good prediction performance during the whole ictal phase. However, seven seizures (No.4, No.6, No.7, No.8, No.16, No.19, No.21) showed a higher incorrect non-EZ detection rate from all the non-EZ electrodes during the first 50 segments after seizure onset. In contrast, six seizures (No.1, No.3, No.10, No.17, No.24, and No.26) displayed a higher incorrect non-EZ detection rate after the 100th segment. Furthermore, two seizures (No.9 and No.23)

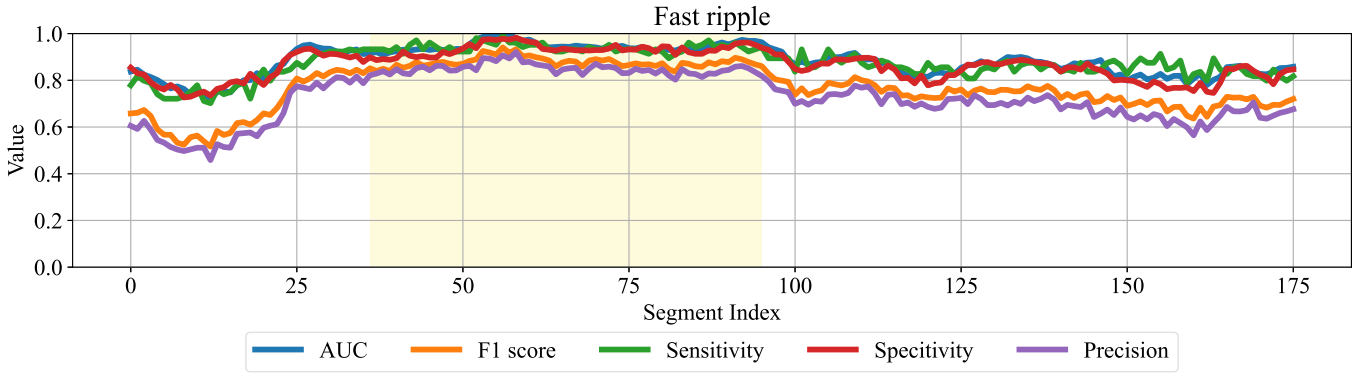

Fig. 3. Global chronological classification evaluations at fast ripple band in the ictal phase for 26 seizures using LightGBM and LOSOCV. X-axis denotes the segment index in the ictal phase. Y-axis represents the evaluation values. Lines with different colors indicate different evaluation matrices. The yellow background denotes the segment range from 23rd to 80th.

exhibited negative predictions for the total segments of the ictal phase.

E. Results of Typical Seizure

It is observed from Supplementary Fig. S7 that seizure No.2 can achieve one of the best predictions, whereas the classification performance of seizure No.9 is the worst. Consequently, we proposed a node-region analysis approach to investigate the time-variant changes of PTE out/in-ratio to investigate the causal connectivity dynamics being sent from an electrode in a given region to another given region for individual seizure. Furthermore, we showed the raw ECoG and chronological normalized PTE out/in-ratio of each electrode for seizures No.2 and No.9. As shown in Supplementary Fig. S8, for seizure No.2, the normalized PTE out/in-ratio values of HPC electrodes increase, whereas the ratio of LTC electrodes decreases in the ictal phase. Moreover, this increase occurs before seizure onset, almost during the last interictal spike. However, there are almost no apparent changes in the out/in-ratio from the interictal to ictal phases for seizure No.9. Furthermore, the videos in Supplementary Fig. S9 and Supplementary Fig. S10 present the chronological changes of the causal influence between pairs of electrodes in the fast ripple band for the representative cases (Seizure No.2 and No.9). In this video, the raw ECoG and corresponding connectogram in fast ripple band were displayed on the left and right sides, respectively. Selected parts surrounded by brown and blue colors are the normalized out/in-ratio in the directions from HPC to LTC (HPC $\rightarrow$ LTC) and from LTC to HPC (LTC $\rightarrow$ HPC), respectively. In addition, the video of seizure No.2 reveals that the directional connectivity values increase from HPC at seizure onset and then spread to LTC. Besides, there exists a decrease in the out/in-ratio exerted from LTC after seizure onset. However, this phenomenon is not prominent, as shown in the video for seizure No.9.

IV. Discussion

We proposed a quantitative causal influence analysis method, which is a unified-epoch PTE-based dynamic analysis method, to investigate the causal influence dynamics of ictal ECoG between connected brain regions (HPC and LTC) with TLE. We demonstrated that it was the most pronounced that the causal influence from HPC exerts to LTC in the ictal phase at the fast ripple band. Based on the overall trend, the time-varying PTE out/in-ratio showed a rise toward the ictal from the interictal phase, with the evaluation of most individual patients acting in accordance with this. In addition, we employed three machine learning models (LightGBM, SVM with linear kernel, and SVM with RBF kernel) and LOSOCV to identify EZ, and we proposed segment-wise and electrodes-wise measures to evaluate the chronological classification performance of individual electrodes. The results showed that the PTE out/in-ratio of electrodes covering in HPC could be a suitable parameter for identifying the EZ.

Effective connectivity is an informative measure to investigate the mechanism of information transmission and process in epileptogenic networks [49]. Standard methods used in studying effective connectivity for TLE include DTF, PDC, TE, and PTE. However, methods such as PDC and DTF rely on the assumption that the signal processed is quasi-stationary and linear. TE and PTE are non-parametric methods and can be used to analyze non-linear and non-stationary signals. However, TE is computationally costly and depends on several prior parameters when compared with PTE [25]. In addition, PTE, as phase-based directed connectivity, is not only robust to noise and mixing linear in EEG, which may result in false positive, but also for large-scale and frequency band-limited analysis [36].

Moreover, for detailed dynamic analysis of the continuous brain interaction time-varying dynamics during a seizure with TLE, the approach of the sliding window with overlapping is introduced in this study. Fig. 2 showed the significant dynamics of two directions, particularly, the prominent changes in fast ripple band in the direction from HPC to LTC. HPC is understood to be the primary region covering electrodes of the seizure onset zone for TLE patients. We illustrated that the strongest PTE out/in-ratio strength occurred in HPC when compared with LTC in gamma and HFOs bands for the ictal phase; thus being in line with the finding of previous literature that the higher causal connectivity values were observed within the epileptic focus for TLE in the ictal state [19], [26].

In addition, to overcome the limitation that the number of electrodes for each patient is varied, we proposed the metric of PTE out/in-ratio to evaluate the information flow for each node and region by summing and taking the average. We subsequently found that the connection difference is more significant in gamma and HFOs bands for two selected regions from Fig. 2. More information was sent than received for HPC in gamma and HFOs bands. Both information from and toward the two regions were strengthened in the ictal phase, whereas the difference in information flow value between regions decreased from the interictal to the ictal phase, suggesting a compensatory mechanism within epileptogenicity [50].

In the statistical analysis, we conducted the FDR corrections to address the potential issue of MCP in the multiple Mann-Whitney U tests comparisons. The FDR correction results revealed that the significance level for the differences in the gamma band between the interictal and ictal phases was reduced compared to the uncorrected p-values. This suggests that the observed differences in the gamma band may not be as robust as initially indicated. Interestingly, our classification results also showed lower accuracy in the gamma band compared to the HFOs bands. This finding aligns with the reduced significance levels in the gamma band indicated by the FDR correction. This indicates that the differences observed in the gamma band may not be as reliably associated with the interictal and ictal phases as the differences observed in the HFOs bands. Overall, the application of FDR corrections allowed us to better control the false positive rate in our statistical analysis and provided a more accurate interpretation of the results. It underscores the importance of considering multiple factors when evaluating the associations between different (frequency, epoch)-pairs and the interictal and ictal phases.

For the evaluation approach, we introduced the LOSOCV to assess the generalization capability of the model by evaluating its performance on unseen seizure data. However, there is a possibility that the model performance may be overestimated if seizure patterns are similar across seizures within a given patient. To address this concern, we also employed the TSNCV to examine the potential impact of within-patient correlations, contributing to a more comprehensive interpretation of the model performance. Our results mitigate the concerns that the LOSOCV measure may result in the accuracy similarities across seizures within a given patient. Future studies are required by expanding the dataset to include more seizures from a diverse set of patients.

The holistic analysis for all 26 seizures exhibits a general pattern of how the directed connectivity changes. We subsequently performed the individual analysis on typical seizures. Our results showed that the HPC sent the most information, consistent with the average global pattern illustrated above. More interestingly, a significant increase in the PTE out/in-ratio originated from HPC at gamma and HFOs bands and a significant decrease sent from LTC below 30 Hz was captured at the seizure onset, indicating a possible sign for predicting seizure onset. In addition, the transient decrease in the PTE out/in-ratio at seizure onset supports the explanation made in the survey that the decreased synchronization at seizure onset correlated to epileptic focus with good outcomes in patients [51].

It has been proposed that seizure occurs due to an imbalance of neural activities between excitation and inhibition [52], [53]. Our findings that more information is sent than received in the HPC during the seizure suggest the disruptions in the excitation-inhibition balance. The imbalance of information flow within the HPC may result in the transmission of excessive neuronal activity and the propagation of the seizure. Furthermore, the findings that the significant increase in the out/in-ratio arose at the middle or end of the seizure support the opinion that except for post-burst inhibition, simultaneous and opposing enhancement of excitation and inhibition contributes to the termination of a focal seizure [54]. It is known that the end of a typical focal seizure is characterized by periodic synchronous bursts with large amplitude [55]. A related survey suggests that the increased neuronal synchronization at the start of the second half of the seizures may promote seizure termination by driving extended neuronal networks simultaneously into a prevention mode [56], sustained by our findings.

However, there are three limitations included in this study. One concern about the findings is a larger number of cases to strengthen generalizability in future research. Besides, regarding the complexity of information flow dynamics at the ictal phase compared to the interictal phase, the ECoG signal at the ictal state is expected to be subdivided into smaller states for further study. Lastly, although the PTE out/in-ratio plays an important role in analyzing the directed connectivity between regions, a comprehensive methodology study would be warranted to interpret the pathological mechanism of various seizures.

V. Conclusion

Understanding the brain connectivity mechanism of TLE seizure among brain regions is challenging research. In this study, we employed the effective connectivity computation method named PTE out/in-ratio to investigate the information transmission dynamics between two selected regions from the interictal to the ictal phase. In addition, we proposed the unified-epoch dynamic analysis methods by introducing the sliding window with overlap on the PTE out/in-ratio to dynamically analyze the connectivity in each small window. More importantly, we employed machine learning algorithms and combined them with LOSOCV to identify EZ. This study mainly entails three findings: 1) Significant increase of the PTE out/in-ratio originating from HPC was observed in gamma and HFOs in the ictal phase when compared to the average interictal PTE out/in-ratio values. 2) In the ictal phase, the significant increase in the PTE out/in-ratio sent by HPC spread across LTC. Simultaneously, the significant increase in the PTE out/in-ratio that originated from LTC occurred in the band range of 10–30 Hz. 3) The classification performance conducted by LightGBM based on the PTE out/in-ratio features at the fast ripple band in the ictal phase outperformed that of another classifier based on the features in the gamma and ripple bands.

Author Contributions

Yao Miao proposed the methodology, programmed, analyzed the ECoG recordings, and wrote the manuscript. Hiroharu Suzuki worked with Yao Miao to give contributions to the methods proposal, data analysis, and manuscript writing. Hidenori Sugano made contributions to improving the methodology, clinical explanation of results, and manuscript. Tetsuya Ueda made contributions to the ECoG data collection and annotation. Yasushi Iimura made contributions to the improvement of the clinical explanation of results and manuscript. Ryosuke Matsui contributed to the built environment of data computation. Toshihisa Tanaka made contributions to the study design, methodology improvement, and manuscript revision.

References

[1] O. Devinsky et al., "Epilepsy," *Nature Rev. Dis. Primers*, vol. 4, 2018, Art. no. 18024.

[2] J. I. Sirven, "Epilepsy: A spectrum disorder," *Cold Spring Harbor Perspectives Med.*, vol. 5, no. 9, 2015, Art. no. a022848.

[3] H. E. Scharfman et al., "Epilepsy as a network disorder: What can we learn from other network disorders such as dementia and schizophrenia, and what are the implications for translational research?," *Epilepsy Behav.*, vol. 78, pp. 106–113, 2018.

[4] R. D. G. Blair, "Temporal lobe epilepsy semiology," *Epilepsy Res. Treat.*, vol. 2012, 2012, Art. no. 751510.

[5] Z. Haneef et al., "Clinical correlates of graph theory findings in temporal lobe epilepsy," *Seizure*, vol. 23, no. 10, pp. 809–818, 2014.

[6] L. Bonilha et al., "Asymmetrical extra-hippocampal grey matter loss related to hippocampal atrophy in patients with medial temporal lobe epilepsy," *J. Neurol., Neurosurgery, Psychiatry*, vol. 78, no. 3, pp. 286–294, 2007.

[7] J. Engel Jr. et al., "Connectomics and epilepsy," *Curr. Opin. Neurol.*, vol. 26, no. 2, 2013, Art. no. 186.

[8] D. J. Englot et al., "Regional and global connectivity disturbances in focal epilepsy, related neurocognitive sequelae, and potential mechanistic underpinnings," *Epilepsia*, vol. 57, no. 10, pp. 1546–1557, 2017.

[9] P. Jiruska et al., "Synchronization and desynchronization in epilepsy: Controversies and hypotheses," *J. Physiol.*, vol. 591, no. 4, pp. 787–797, 2013.

[10] F. Pittau et al., "Mapping epileptic activity: Sources or networks for the clinicians?," *Front. Neurol.*, vol. 5, 2014, Art. no. 218.

[11] M. A. Kramer et al., "Epilepsy as a disorder of cortical network organization," *Neuroscientist*, vol. 18, no. 4, pp. 360–372, 2012.

[12] C. G. Reddy et al., "Decoding movement-related cortical potentials from electrocorticography," *Neurosurgical Focus*, vol. 27, no. 1, 2009, Art. no. E11.

[13] K. J. Friston, "Functional and effective connectivity in neuroimaging: A synthesis," *Hum. Brain Mapping*, vol. 2, no. 1-2, pp. 56–78, 1994.

[14] C. W. J. Granger, "Investigating causal relations by econometric models and cross-spectral methods," *Econometrica*, vol. 37, no. 3, pp. 424–438, 1969.

[15] L. A. Baccalá et al., "Partial directed coherence: A new concept in neural structure determination," *Biol. Cybern.*, vol. 84, pp. 463–474, 2001.

[16] M. J. Kamiński et al., "A new method of the description of the information flow in the brain structures," *Biol. Cybern.*, vol. 65, pp. 203–210, 1991.

[17] P. J. Franaszczuk et al., "Analysis of mesial temporal seizure onset and propagation using the directed transfer function method," *Electroencephalogr. Clin. Neuriophysiol.*, vol. 91, no. 6, pp. 413–427, 1994.

[18] P. J. Franaszczuk et al., "Application of the directed transfer function method to mesial and lateral onset temporal lobe seizures," *Brain Topogr.*, vol. 11, no. 1, pp. 13–21, 1998.

[19] C. Wilke et al., "Identification of epileptogenic foci from causal analysis of ECoG interictal spike activity," *Clin. Neuriophysiol.*, vol. 120, no. 8, pp. 1449–1456, 2009.

[20] P. van Mierlo et al., "Accurate epileptogenic focus localization through time-variant functional connectivity analysis of intracranial electroencephalographic signals," *NeuroImage*, vol. 56, no. 3, 2011, pp. 1122–1133.

[21] P. van Mierlo et al., "Ictal-onset localization through connectivity analysis of intracranial EEG signals in patients with refractory epilepsy," *Epilepsia*, vol. 54, no. 8, pp. 1409–1418, 2013.

[22] C. M. Epstein et al., "Application of high-frequency Granger causality to analysis of epileptic seizures and surgical decision making," *Epilepsia*, vol. 55, no. 12, pp. 2038–2047, 2014.

[23] C. Wilke, L. Ding, and B. He, "Estimation of time-varying connectivity patterns through the use of an adaptive directed transfer function," *IEEE Trans. Biomed. Eng.*, vol. 55, no. 11, pp. 2557–2564, Nov. 2008.

[24] T. Schreiber, "Measuring information transfer," *Phys. Rev. Lett.*, vol. 85, no. 2, 2000, Art. no. 461.

[25] M. Lobier et al., "Phase transfer entropy: A novel phase-based measure for directed connectivity in networks coupled by oscillatory interactions," *NeuroImage*, vol. 85, pp. 853–872, 2014.

[26] M. Y. Wang et al., "Identification of the epileptogenic zone of temporal lobe epilepsy from stereo-electroencephalography signals: A phase transfer entropy and graph theory approach," *NeuroImage: Clin.*, vol. 16, pp. 184–195, 2017.

[27] J. Engel, "Update on surgical treatment of the epilepsies," *Neurology*, vol. 43, no. 8, pp. 1612–1612, 1993.

[28] C. Tonini et al., "Predictors of epilepsy surgery outcome: A meta-analysis," *Epilepsy Res.*, vol. 62, no. 1, pp. 75–87, 2004.

[29] A. Delorme et al., "EEGLAB: An open-source toolbox for analysis of single-trial EEG dynamics," *J. Neurosci. Methods*, vol. 134, no. 1, pp. 9–21, 2004.

[30] I. V. Blagouchine and E. Moreau, "Analytic method for the computation of the total harmonic distortion by the Cauchy method of residues," *IEEE Trans. Commun.*, vol. 59, no. 9, pp. 2478–2491, Sep. 2011.

[31] A. Hillebrand et al., "Direction of information flow in large-scale resting-state networks is frequency-dependent," *Proc. Nat. Acad. Sci. United States Amer.*, vol. 113, no. 14, pp. 3867–3872, 2016.

[32] N. Wiener, "The theory of prediction," in *Modern Mathematics for the Engineer: First Series*, E. F. Beckenbach, Ed. New York, NY,USA: Doubleday, 1956, pp. 165–190.

[33] C.-Z. Yao et al., "Effective transfer entropy approach to information flow among EPU, investor sentiment and stock market," *Front. Phys.*, vol. 8, pp. 1–14, 2020.

[34] D. W. Scott, *Multivariate Density Estimation*. New York, NY,USA: Wiley, 1992.

[35] N. I. Fisher, *Statistical Analysis of Circular Data*. Cambridge, U.K.: Cambridge Univ. Press, 1996.

[36] G. M. Bidelman et al., "Afferent-efferent connectivity between auditory brainstem and cortex accounts for poorer speech-in-noise comprehension in older adults," *Hear. Res.*, vol. 382, 2019, Art. no. 107795.

[37] R. Janca et al., "Ictal gamma-band interactions localize ictogenic nodes of the epileptic network in focal cortical dysplasia," *Clin. Neuriophysiol.*, vol. 132, no. 8, pp. 1927–1936, 2021.

[38] A. Vargha et al., "A critique and improvement of the CL common language effect size statistics of McGraw and Wong," *J. Educ. Behav. Statist.*, vol. 25, no. 2, pp. 101–132, 2000.

[39] M. Tomczak et al., "The need to report effect size estimates revisited. An overview of some recommended measures of effect size," *Trends Sport Sci.*, vol. 1, no. 21, pp. 19–25, 2014.

[40] P. J. Durka et al., "On the statistical significance of event-related EEG desynchronization and synchronization in the time-frequency plane," *IEEE Trans. Biomed. Eng.*, vol. 51, no. 7, pp. 1167–1175, Jul. 2004.

[41] Y. Benjamini et al., "Controlling the false discovery rate: A practical and powerful approach to multiple testing," *J. Roy. Stat. Soc.: Ser. B. (Methodological)*, vol. 57, pp. 289–300, 1995.

[42] G. Ke et al., "LightGBM: A highly efficient gradient boosting decision tree," in *Proc. Adv. Neural Inf. Process. Syst.*, 2017, pp. 3146–3154.

[43] B. Kanber et al., "Detection of covert lesions in focal epilepsy using computational analysis of multimodal magnetic resonance imaging data," *Epilepsia*, vol. 62, no. 3, pp. 807–816, 2021.

[44] Y. Miao et al., "Seizure onset zone identification using phase-amplitude coupling and multiple machine learning approaches for interictal electrocorticogram," *Cogn. Neurodynamics*, pp. 1–17, 2022.

[45] M. S. Akter et al., "Statistical features in high-frequency bands of interictal ieeg work efficiently in identifying the seizure onset zone in patients with focal epilepsy," *Entropy*, vol. 22, no. 12, 2020, Art. no. 1415.

[46] Microsoft, "LightGBM: LightGBM Python package," 2023. [Online]. Available: https://github.com/microsoft/LightGBM

[47] C. Cortes et al., "Support-vector networks," *Mach. Learn.*, vol. 20, no. 3, pp. 273–297, 1995.

[48] Y. Varatharajah et al., "Integrating artificial intelligence with real-time intracranial EEG monitoring to automate interictal identification of seizure onset zones in focal epilepsy," *J. Neural Eng.*, vol. 15, no. 4, 2018, Art. no. 046035.
[49] J. J. Bear et al., "The epileptic network and cognition: What functional connectivity is teaching us about the childhood epilepsies," *Epilepsia*, vol. 60, no. 8, pp. 1491–1507, 2019.
[50] G. Bettus et al., "Decreased basal fMRI functional connectivity in epileptogenic networks and contralateral compensatory mechanisms," *Hum. Brain Mapping*, vol. 30, no. 5, pp. 1491–1507, 2009.
[51] S. P. Burnsa et al., "Network dynamics of the brain and influence of the epileptic seizure onset zone," *Proc. Nat. Acad. Sci.*, vol. 111, no. 49, pp. E5321–E5330, 2014.
[52] R. A. B. Badawy et al., "Epilepsy: Ever-changing states of cortical excitability," *Neuroscience*, vol. 11, no. 222, pp. 89–99, 2012.
[53] X. Dai et al., "Brain network excitatory/inhibitory imbalance is a biomarker for drug-naive rolandic epilepsy: A radiomics strategy," *Epilepsia*, vol. 62, no. 10, pp. 2426–2438, 2021.
[54] D. Boido et al., "Simultaneous enhancement of excitation and postburst inhibition at the end of focal seizures," *Ann. Neurol.*, vol. 76, no. 6, pp. 826–836, 2014.
[55] R. Fisher et al., "How can we identify ictal and interictal abnormal activity?," *Adv. Exp. Med. Biol.*, vol. 813, pp. 3–23, 2014.
[56] K. Schindler et al., "Increasing synchronization may promote seizure termination: Evidence from status epilepticus," *Clin. Neuriophysiol.*, vol. 118, no. 9, pp. 1955–1968, 2007.